

COMPARISON OF RECONSTRUCTION METHODS FOR COMPUTERIZED TOMOGRAPHY

Vítězslav Vít VLČEK¹

Abstract: This article deals with a brief description of two basic algorithms for computation of the inverse Radon transform (Fourier Method and FBP). The rest of this article is devoted to the comparison of the FBP and a new method for computation of the inverse Radon transform which is based on solving PDE. This new method is more time expensive than FBP but it produces significantly better outputs than FBP.

Keywords: Filtered Back Projection, Inverse Radon Transform, Total Variation.

1 INTRODUCTION

The inverse Radon transform is used in many fields, especially in the Computerized Tomography (CT). Current CT scanners use a common method for computation of inverse Radon transform which is called Filtered Back Projection (FBP). This method is very fast since it is based on 1D and 2D Fast Fourier Transform (FFT) but it also has some caveats which I want to describe later. Therefore I decided to develop a new method for computation of the inverse Radon transform, which is based on the discrete approximation of the direct Radon transform and on minimizing total variation of the reconstructed image.

2 COMPUTERIZED TOMOGRAPHY AND RADON TRANSFORM

The first generation of the CT scanners had the simplest form (see Figure 3.1, for other CT scanner generation see http://en.wikipedia.org/wiki/Computed_tomography). The X-ray tube produced an X-ray beam which was able to pass through a soft tissue in human body. But there were also some harder parts of human body where X-ray was absorbed, for instance bones. The detector measured an intensity of X-ray in the direction of X-ray tube, after that both X-ray tube and detector were shifted for a small step in the same direction (for instance from left to right, see Figure 3.1 for translation movement) and then X-ray tube emitted beam again and detector measured X-ray intensity. When both detector and X-ray tube performed all scans in the same direction, then they were rotated (the center of rotation is in the center of scanned object, see Figure 3.1 for rotation movement) and the whole process of measuring was carried out again. The rotation of detector and X-ray tube was performed around whole scanned object. The process of image reconstruction could start once data were collected. The result of the image reconstruction displays attenuation coefficients in gray levels.

The intensity of X-ray beam changes according to environment by which the beam goes through. For instance, we have homogenies tissue with specified constant μ_1 , which we call attenuation coefficient. The measured intensity of detected X-ray beam is driven by exponential decay of the form

$$I(\theta, t) = I_0 e^{-\mu_1 s_1(\theta, t)},$$

where I_0 is the intensity of emitted beam, $s_1(\theta, t)$ is the length of intersection of X-ray beam with homogenies tissue and θ, t depend on the particular position of detector and X-ray tube. For two tissues with different attenuation coefficients μ_1, μ_2 we get

$$I(\theta, t) = I_0 e^{-\mu_1 s_1(\theta, t)} e^{-\mu_2 s_2(\theta, t)} = I_0 e^{-(\mu_1 s_1(\theta, t) + \mu_2 s_2(\theta, t))}.$$

¹Ing. Vítězslav Vít VLČEK, University of West Bohemia in Pilsen, Faculty of Applied Sciences, Department of Mathematics, Univerzitní 22, 306 14 Pilsen, tel.: +420 377632660, e-mail: vsoft@kma.zcu.cz

And finally, for a non-homogenies tissue we get

$$I(\theta, t) = I_0 e^{-\int_{\Omega=\{\mathbf{x} \in \mathbb{R}^2: \boldsymbol{\theta}^T \mathbf{x}=t\}} \mu(\mathbf{x}) d\mathbf{x}}. \quad (2.1)$$

So we know an emitted intensity of the X-ray beam I_0 , further we also know intensity of the detected X-ray beam (2.1) and we want to know the attenuation (coefficients) function $\mu(\mathbf{x})$. We start out from (2.1), do some calculation and we get

$$\ln \frac{I_0}{I(\theta, t)} = \int_{\Omega=\{\mathbf{x} \in \mathbb{R}^2: \boldsymbol{\theta}^T \mathbf{x}=t\}} \mu(\mathbf{x}) d\mathbf{x} = \mathcal{R} \{ \mu \} (\theta, t), \quad (2.2)$$

where the term $\int_{\Omega=\{\mathbf{x} \in \mathbb{R}^2: \boldsymbol{\theta}^T \mathbf{x}=t\}} \mu(\mathbf{x}) d\mathbf{x}$ is called the Radon transform of $\mu(\mathbf{x})$. The vector $\boldsymbol{\theta}$ is a member of the set \mathcal{S}^1 . The set $\mathcal{S}^1 = \{ \mathbf{y} \in \mathbb{R}^2 : \mathbf{y}^T \mathbf{y} = 1 \}$ contains all unit vectors of \mathbb{R}^2 , for example $\boldsymbol{\theta} = [\cos \theta, \sin \theta]^T$. If we want to get the unknown attenuation coefficients $\mu(\mathbf{x})$ we have to perform the inverse Radon transform of the term $\ln \frac{I_0}{I(\theta, t)} = \hat{\mu}(\theta, t)$, i.e.

$$\mu(\mathbf{x}) = \mathcal{R}^{-1} \{ \hat{\mu}(\theta, t) \} = \mathcal{R}^{-1} \left\{ \ln \frac{I_0}{I(\theta, t)} \right\}. \quad (2.3)$$

And there is at least one caveat when $I(\theta, t) = 0$.

3 THE CLASSIC METHODS FOR INVERSE RADON TRANSFORM

The first method for computation of the Inverse Radon Transform is called the Fourier Method. This method is based on the Fourier Slice Theorem.

Theorem 3.1 Let the functions $F(\theta, t)$, $f(x_1, x_2)$ satisfy the condition $F = \mathcal{R} \{ f \}$ then it holds

$$\mathcal{F} \{ F(\theta, t) \} (v) = \mathcal{F} \{ f(x_1, x_2) \} (v \cos \theta, v \sin \theta) \quad \forall v \in \mathbb{R}, \theta \in [0, \pi[. \quad (3.4)$$

The 1D Fourier transform of a Radon projection taken at angle θ equals the central radial slice at angle θ of the 2D Fourier transform of the original object. For graphics meaning, see Fig. 3.1.

If we use the Fourier Slice Theorem and replace the Fourier transform by the Discrete

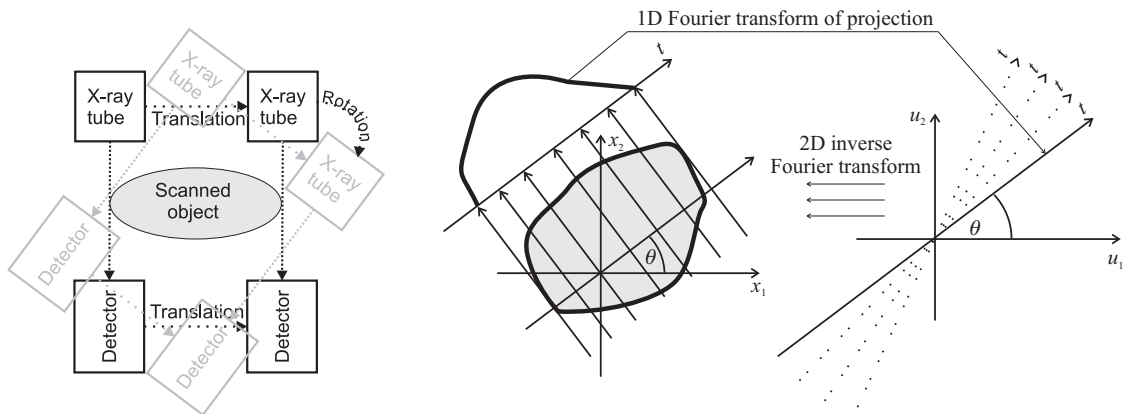


Fig. 3.1: The left-hand figure shows the scheme of the CT scanner of the first generation, the right-hand figure displays the relation between 2D Fourier spectrum and Radon spectrum – the graphic meaning of the Fourier Slice Theorem 3.1.

Fourier Transform (DFT) then we get the Fourier Method – see Fig. 3.1.

But there are some troubles from the numerical point of view since the density of the radial points becomes sparser as one gets farther away from the center and the interpolation error also becomes larger. This implies that there is larger error in the calculation of the high frequency components of the image than in that of the low frequency ones, which results in individual image degradation (Sla87), pages 59-60 – see Fig. 3.2. The Fourier Method and its numerical implementation is described more precisely in (Tof96), pages 116-121.

3.1 Filtered Back Projection

This algorithm uses the Fourier Slice Theorem, too, but it tries to remove the problem with the interpolation error which was described in the previous section. If we express the inverse 2D Fourier transform in the polar coordinates we get the FBP. We start out from

$$f(x_1, x_2) = \mathcal{F}^{-1}\{F(t_1, t_2)\}(x_1, x_2) = \int_{-\infty}^{\infty} \int_{-\infty}^{\infty} e^{i2\pi(x_1 t_1 + x_2 t_2)} F(t_1, t_2) dt_1 dt_2. \quad (3.5)$$

$$t_1 = v \cos \theta$$

After using the substitution $t_2 = v \sin \theta$ we get further $dt_1 dt_2 = v dv d\theta$

$$f(x_1, x_2) = \int_0^{2\pi} \int_0^{\infty} F(v \cos \theta, v \sin \theta) v e^{i2\pi v(x_1 \cos \theta + x_2 \sin \theta)} dv d\theta \quad (3.6)$$

$$= \int_0^{\pi} \left(\int_{-\infty}^{\infty} M(\theta, v) |v| e^{i2\pi v(x_1 \cos \theta + x_2 \sin \theta)} dv \right) d\theta \quad (3.7)$$

$$= \int_0^{\pi} \hat{m}(\theta, x_1 \cos \theta + x_2 \sin \theta) d\theta, \quad (3.8)$$

where $\hat{m}(\theta, t) = \int_{-\infty}^{\infty} M(\theta, v) |v| e^{i2\pi vt} dv$. The multiplication by $|v|$ serves as a filter applied to each projection in the Fourier spectrum. For the numerical implementation see (Tof96), pages 111-114.

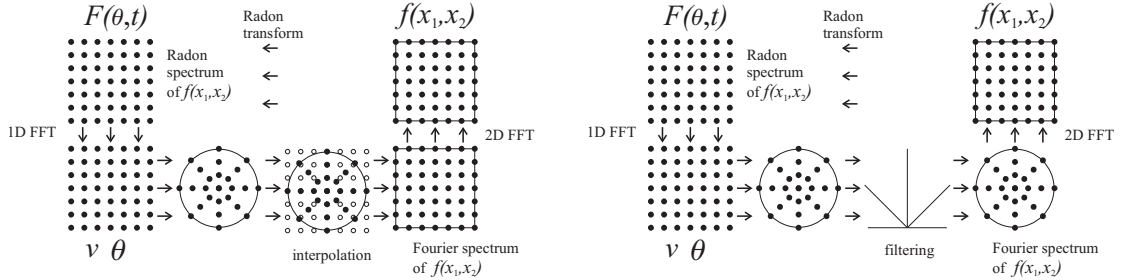


Fig. 3.2: The left-hand figure displays computation scheme of the Fourier Method, the right-hand figure shows the scheme of the Filtered Back Projection.

4 A NEW METHOD FOR THE INVERSE RADON TRANSFORM

The reconstruction of the function u (a reconstructed image) from a function \hat{u} (measured data by the CT scanner) is given by the formula $u = \mathcal{R}^{-1}\{\hat{u}\}$. My new method for computation of the inverse Radon transform \mathcal{R}^{-1} is based on the minimization of a functional F_α . A classical way to overcome ill-posed tasks is to add a regularization term. The functional for computation of the inverse Radon transform has the form

$$F_\alpha(u) = \frac{1}{2} \int_{\Omega} (Ku - \hat{u})^2 d\mathbf{x} + \alpha \int_{\Omega} R(|\nabla u|) d\mathbf{x}, \quad \mathbf{x} = [x_1, x_2]^T, \Omega = \mathbb{R}^2, \quad (4.9)$$

where the first term in $F_\alpha(u)$ deals with data fidelity, $\alpha \in [0, \infty[$ is a weight of the regularization term and $R(|\nabla u|) = R(\sqrt{u_x^2 + u_y^2})$, $R : \mathbb{R}^+ \rightarrow \mathbb{R}^+$, is the regularization function. If we put $\alpha = 0$, we get $F_0(u) = \frac{1}{2} \int (Ku - \hat{u})^2 d\mathbf{x}$. The task to find $\inf F_0(u)$ is identical with the equation $K^*Ku = K^*\hat{u}$, where K^* is the adjoint operator to K . Unfortunately, we cannot usually perform the inversion of K^*K since the solution u does not depend continuously on the initial data. Hence we call this task ill-posed. That is the reason why we need the regularization term $\alpha > 0$.

Functional $F_\alpha(u)$ has the form $\int_{-\infty}^{\infty} \int_{-\infty}^{\infty} G(x_1, x_2, u, u_{x_1}, u_{x_2}) dx_1 dx_2$. The condition for the stationary point of this functional is $\delta F_\alpha(u, h) = 0 \quad \forall h \in X_0$ which leads us to the Euler-Lagrange equation

$$\frac{\partial F_\alpha}{\partial u} - \frac{\partial}{\partial x} \frac{\partial F_\alpha}{\partial u_{x_1}} - \frac{\partial}{\partial y} \frac{\partial F_\alpha}{\partial u_{x_2}} = 0. \quad (4.10)$$

We put (4.9) into the Euler-Lagrange equation (4.10) and we get

$$(K^*Ku - K^*\hat{u}) - \alpha \operatorname{div} \left(\frac{R'(|\nabla u|) \nabla u}{|\nabla u|} \right) = 0, \quad (4.11)$$

$$u_n = 0.$$

If we choose $R(\tau) = \tau$, $R'(\tau) = 1$, then we obtain the equation

$$(K^*Ku - K^*\hat{u}) - \alpha \operatorname{div} \left(\frac{\nabla u}{|\nabla u|} \right) = 0, \quad (4.12)$$

$$u_n = 0.$$

If we choose $R(\tau) = \frac{\tau^2}{2}$, $R'(\tau) = \tau$, then we obtain the equation

$$(K^*Ku - K^*\hat{u}) - \alpha \Delta u = 0, \quad (4.13)$$

$$u_n = 0.$$

These PDEs are frequently used in denoising and deblurring tasks. The Computerized Tomography can be connected with these tasks by the operator K . The operator K represents the direct Radon transform. The deblurring of the image means to perform the inverse Radon transform. According to (Ma99) it is better to solve (5.14) than (4.12), since (5.14) reaches steady state earlier than (4.12).

5 NUMERICAL IMPLEMENTATION OF NEW METHOD

I decided to use an explicit numerical scheme (see (Ma99)) for the discretisation of the following partial differential equation

$$\frac{\partial u}{\partial t} = |\nabla u| \left(\alpha \operatorname{div} \left(\frac{\nabla u}{|\nabla u|} \right) - K^*(Ku - \hat{u}) \right) \quad \text{for } \mathbf{x} \in \Omega, t \in (0, T),$$

$$\frac{\partial u}{\partial n} = 0 \quad \text{for } \mathbf{x} \in \partial\Omega, t \in (0, T), \quad (5.14)$$

$$u(0, \mathbf{x}) = g(\mathbf{x}) \quad \text{for } \mathbf{x} \in \Omega,$$

where the operator K represents the Radon transform. The functions $\hat{u} \neq g$ since the function \hat{u} represents measured data by the CT scanner while the function g represents an initial guess of the reconstructed function $u(\mathbf{x})$. The function $g(\mathbf{x})$ can be a constant function (for example a zero function) or it is usually better to take a result of a fast method for the computation of the inverse Radon transform as an initial guess (for example

the result of the Filtered Back Projection). The discretisation of the individual terms gives (assume $\Delta x = \Delta y = 1$)

$$u_{ij}^n = u(n\Delta t, i\Delta x, j\Delta y) = u(n\Delta t, i, j), \quad (5.15)$$

$$g_{ij} = g(i\Delta x, j\Delta y) = g(i, j), \quad (5.16)$$

$$\hat{u}_{ij} = \hat{u}(i\Delta x, j\Delta y) = \hat{u}(i, j), \quad (5.17)$$

$$\frac{\partial u}{\partial t} \approx \frac{u_{ij}^{n+1} - u_{ij}^n}{\Delta t}, \quad (5.18)$$

$$|\nabla u| \left(\alpha \operatorname{div} \left(\frac{\nabla u}{|\nabla u|} \right) \right) = \begin{cases} \alpha \frac{u_{xx}u_y^2 - 2u_{xy}u_xu_y + u_{yy}u_x^2}{u_x^2 + u_y^2} & \text{for } u_x^2 + u_y^2 \geq \beta, \\ 0 & \text{elsewhere,} \end{cases} \quad (5.19)$$

where the term (5.19) is discretised by central differences:

$$u_{xx} \approx u_{i+1,j}^n - 2u_{ij}^n + u_{i-1,j}^n, \quad u_{yy} \approx u_{i,j+1}^n - 2u_{ij}^n + u_{i,j-1}^n, \quad (5.20)$$

$$u_x \approx \frac{u_{i+1,j}^n - u_{i-1,j}^n}{2}, \quad u_y \approx \frac{u_{i,j+1}^n - u_{i,j-1}^n}{2}, \quad (5.21)$$

$$u_{xy} \approx \frac{u_{i+1,j+1}^n - u_{i-1,j+1}^n - u_{i+1,j-1}^n + u_{i-1,j-1}^n}{4}, \quad (5.22)$$

and the following term is discretised by the upwind differences

$$-|\nabla u| (K^*(Ku - \hat{u})) = -\sqrt{(u_x^\pm)^2 + (u_y^\pm)^2} (K^*(Ku - \hat{u})), \quad (5.23)$$

where if $u_x (K^*(Ku - \hat{u})) > 0$ then

$$u_x^\pm \approx u_{ij}^n - u_{i-1,j}^n, \quad (5.24)$$

if $u_x (K^*(Ku - \hat{u})) \leq 0$ then

$$u_x^\pm \approx u_{i+1,j}^n - u_{ij}^n, \quad (5.25)$$

if $u_y (K^*(Ku - \hat{u})) > 0$ then

$$u_y^\pm \approx u_{ij}^n - u_{i,j-1}^n, \quad (5.26)$$

if $u_y (K^*(Ku - \hat{u})) \leq 0$ then

$$u_y^\pm \approx u_{i,j+1}^n - u_{ij}^n. \quad (5.27)$$

The values of the functions u, \hat{u}, g are stored in computer memory as vectors since it is very easy to perform $R^*(Ru - \hat{u})$.

6 NUMERICAL EXPERIMENTS

I performed a numerical experiment with the new method and I compared results with the classic method for the computation of the inverse Radon transform (FBP). I used modified Shepp-Logan head phantom of size 128×128 . The Radon transform of this phantom had 180 angular and 250 translate projections (see Fig. 6.3). The parameters for the numerical simulation were $\Delta t = 9.1 \cdot 10^{-4}$, $\alpha = \frac{1}{7}$, $\beta = 10^{-6}$. The comparison of the results of the FBP with the new method is shown in Fig. 6.3.

Method	Computation Time	Max error
FBP	1 s	261
New method	280 s = 400 iterations	12

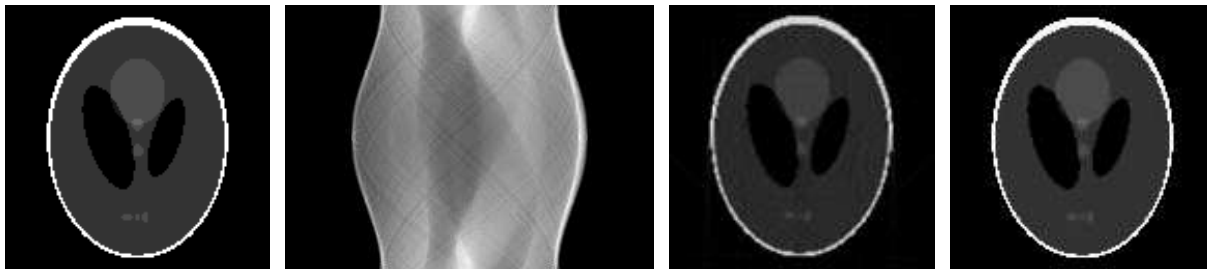


Fig. 6.3: The first picture displays the original test image of size 128×128 . It is famous modified Shepp-Logan head phantom that is usually used for simulations (see Matlab command `phantom`). The second picture shows sinogram (180 angular projections and 250 translate projections), i.e. the Radon transform of the source (the first) image. It is CT scanner simulation of the original image (see Matlab command `radon`). The third picture displays the reconstruction by the Filtered Back Projection. The last picture shows the reconstruction done by the new method.

The second column of the previous table shows CPU time, the third column shows maximal error, i.e. $\max_{\Omega}(|\text{Original Image} - \text{Restored Image}|)$. For the original image see Fig. 6.3.

7 CONCLUSION

We can see in the comparison table that the computation time of the new method is very long. The reason why it is so is the following: at first the FBP is a part of Matlab hence it is optimized in C language, further the FBP is based on the FFT and 2D FFT. The new method is entirely composed in Matlab language and its code is more complex than FBP hence it is slow. But the experiments show that the new method is more flexible, it can handle more CT scanner geometries, it can better treat noise in data, it gives more precise and smoother results than the FBP.

This method can be extended in the following way: better approximation of the direct Radon transform (operator K), the explicit numerical scheme can be of the second order and finally, the whole method can be rewritten in C language for bigger speedup.

REFERENCES

- [Nat86] Natterer, F., 1986. *The mathematics of computerized tomography*. USA, SIAM, ISBN 0-89871-493-1 (pbk.), preprint published by Wiley in 1986.
- [Sla87] Slaney, M., Kak, A.C., 1999. *Principles of computerized tomographic imaging*. USA, IEEE Press, ISBN 0-87942-198-3, <http://www.slaney.org>.
- [Tof96] Toft, P., 1996. *The Radon transform, theory and implementation*. Ph.D. thesis, Technical University of Denmark, <http://petertoft.dk/PhD>.
- [Aub00] Aubert, G., Kornprobst, P., 2000. *Mathematical Problems in Image Processing*. Springer, ISBN 0-387-95326-4.
- [Ma99] Marquina, A., Osher, S., 1999. *Explicit Algorithms for a New Time Dependent Model Based on Level Set Motion for Nonlinear Deblurring and Noise Removal*. <ftp://ftp.math.ucla.edu/pub/camreport/cam99-5.ps.gz>.